JOURNAL OF MATERIALS SCIENCE: MATERIALS IN MEDICINE **17** (2006) 15–27

Effect of passivation and surface modification on the dissolution behavior and nano-surface characteristics of Ti-6Al-4V in Hank/EDTA solution

T. M. LEE
Institute of Oral Medicine, National Cheng Kung University, Tainan 701, Taiwan
E-mail: tmlee@mail.ncku.edu.tw.

The aim of the present study was to investigate the effects of passivation treatment (34% nitric acid passivation, 400 °C heated in air, and aged in 100 °C de-ionized water) and surface modification (2 hr and 8 hr vacuum-brazed treatments) on the ion dissolution and nano-surface characteristics of Ti-6Al-4V exposed in Hank's solution with 8.0 mM ethylene diamine tetra-acetic acid (EDTA) at 37 °C. The results indicated that the original nano-surface characteristics and microstructure would influence the ion dissolution but not change the capability of the Ca and P adsorption upon immersion. Of the three passivated treatments, 400 °C thermal treatment for both 2 hr brazed Ti-6Al-4V (B2) and 8 hr brazed Ti-6Al-4V (B8) exhibits a substantial reduction in the constituent release compared to the acid passivated and water aged treatment, because the thicker thickness and rutile structure of surface oxide could provide the better dissolution resistance for 400 °C-treated specimens. Moreover, the reduced Ti_2Cu and increased α-titanium structure in B8 specimen could also improve ion dissolution resistance in comparison with B2 specimen. After soaking in Hank/EDTA solution, the adsorbed non-elemental Ca and P for all groups of specimens were observed by XPS analysis, and the AES depth-profile analysis indicate that the oxide films of all groups of specimens thicken with the longer immersion periods. The increasing oxide thickness may be the factor in the improved dissolution resistance at the longer immersion periods. The relation between lower dissolution rate and thicker oxide films were observed for all groups of specimens. The results suggest that the dissolution kinetics was governed by the metal ion transport through the oxide film in this study.

1. Introduction

The clinical use of titanium or its alloy on dental and orthopedic implant has been increasing owing to their relatively excellent corrosion and favorable biocompatibility, compared to stainless steel and cobalt chromium alloys [1, 2]. The reasons for the apparent success of titanium or its alloy implants have been attributed to the existence of a thin, stable passivating oxide layer of TiO_2. Albrektsson *et al*. and Kasemo *et al*. mentioned that the biocompatibility of titanium implants is associated with the surface titanium oxide not with the titanium metal [2, 3]. Several investigations reported that the surface topography and roughness of titanium and its alloy have been shown to be the important factors in controlling the shape, orientation, and adhesion of cell. However, few studies have investigated the effect of nano-surface characteristics and ion dissolution on the biocompatibility and cytocompatibility.

In clinical use, the implant material surface is in intimate contact with the living tissue and its biocompatibility is determined in large part by the surface properties of the materials, which have a direct effect on the cellular response to the materials. The oxide film of titanium or its alloy has been known to have at least two types of hydroxyl groups, basic and acidic OH, attached to it by chemisorption. The acidic hydroxyl groups tend to act as cation exchange sites, while basic hydroxyl groups may act as anion exchanges sites [3–8]. These may in turn react with calcium and phosphate binding biomolecules to provide a gradual transition from the metal to living cells [9], which may be important for the osseointegration behavior of titanium

and its alloy implants. Meanwhile, the ion releases of titanium metal are mainly determined by the properties of oxide films [10, 11]. The different levels of ion release would change the environmental fluid condition and further influence the reaction between the cell and implant.

A dissolution of titanium through the oxide into the solution has been proposed as being responsible for the titanium ion release [12–14]. Browne and Gregson and Wisbey *et al.* have used the different passivation methods to investigate the dissolution behavior of titanium [10, 11], and their results indicate that the structure of surface oxide would change the dissolution rate. Recently, we have examined the influence of chemistries and surface characteristics of T-i6Al-4V on the adsorption of Ca and P species and ion dissolution behavior of the material. The results indicate that passivation influences the surface oxide thickness and the early stage ion dissolution rate of the alloy [15]. The rate-limiting step of the dissolution rate can be best explained by the metal ion transport through the oxide film, rather than hydrolysis of the film. Variation of the chemistries of titanium alloy alters the electromotive force potential of the metal, thereby affecting the corrosion and ion dissolution rate.

The fixation by mechanical interlocking of porous implant coatings and bone tissue ingrowth into the pores have extended significantly after 1980s [16–19]. In order to fabricate porous-coated device suitable for bone ingrowth, Ti6Al4V alloy systems must be heat treated above the beta transus (992 °C) [17, 18, 20, 21]. Typically, the particles (wire or powder) are sintered at 1250 °C for 1 to 3 h in a nonoxidizing atmosphere (vacuum or very pure inert gas). Such treatment at high temperature results in a transformation from equiaxed grain, suggested for surgical implants, to lamellar alpha-beta microstructure, which will seriously decrease the fatigue properties of Ti6Al4V alloy [20–23]. For solving the mechanical properties of titanium base alloy, the vacuum brazing method have been applied to manufacture the porous coating below the beta transus, and the endurance limit of porous coated Ti6Al4V alloy, under axial loading condition, was 215 MPa in comparison with 105 MPa by conventional sintering method (1300 °C) [24]. By X-ray diffractometry (XRD), the phase of Ti_2Cu were identified in the vacuum-brazed Ti6Al4V, and the electrochemical behavior of Ti_2Cu bulk specimens show worse corrosion resistance than commercial pure (CP) Ti and Ti6Al4V in oxygen-saturated Hank's solution [25]. The change in microstructure of the brazed Ti6Al4V was as a function of brazing time, and the increasing heat-treated period from 2 h (B2 specimen) to 8 h (B8 specimen) can significantly decrease the quantity of Ti_2Cu and increase the content of α-titanium structure by XRD.

In the present study, the B2 and B8 specimens was adopted to investigate the effect of microstructure on the ion dissolution and nano-surface characteristics of materials (Ti-6Al-4V) exposed to Hank's solution with 8.0 mM ethylene diamine tetra-acetic acid (EDTA) at 37 °C. Besides, three different passivation treatments (34% nitric acid passivation, 400 °C heated in air, and aged in 100 °C de-ionized water) are also adopted to investigate the effect of original nano-surface characteristics on the ion dissolution and nano-surface characteristics after soaking in Hank/EDTA solution.

2. Materials and methods

2.1. Experimental materials and passivation treatment

To prepare specimens, titanium-base filler metal (Ti-15Cu-15Ni, m.p. 934 °C) of 50 μm in thickness were placed on 12.7 mmϕ × 2.0 mm Ti-6Al-4V alloy (ASTM F136-92) substrate and heat treated in a high-temperature furnace with a vacuum pressure less than 10^{-5} Torr. Two kinds of experimental materials used in this study were: (a) Ti-6Al-4V alloy brazed at 970 °C for 2 h (B2) and (b) Ti-6Al-4V brazed at 970 °C for 8 h (B8). The brazed Ti-6Al-4V were ground through successive silicon carbide papers to 1500 grit, then subjected to sonication in acetone and rinsed three times in double distilled water. After polishing and cleaning, both B2 and B8 materials was passivated by the following procedure:(a) immersed in 34% nitric acid for 1 hr (P), (b) 400 °C in air for 45 min (T), and (c) aging in boiling de-ionized water for 24 h (A). After passivation, the passivated samples are referred with P, T or A adding to the notations for experimental materials. Thus, six groups of specimens consisting of B2P, B2T, B2A, B8P, B8T, and B8A were prepared. After passivation treatment, the specimens were autoclaved and sterilized with steam at 121 °C for 30 min and dried at 121 °C for 15 min.

2.2. Immersion protocol

After passivation and autoclave treatments, eight specimens for each of the six groups were immersed in Hank's solution with 8.0 mM ethylene diamine tetra-acetic acid (EDTA) at 37 °C. The eight specimens in each of the six groups were placed individually in the sterilized bottles with a surface area to solution volume ratio of 0.1 cm^{-1}. Additional control groups consisted of bottles with an identified volume of test solution, but without specimens. The differential immersion experiments were selected by exchanging the test solution periodically. For each time period (1, 2, 4, 8, 16, and 32 days), the incubated medium was poured from each bottles into a cleaned and labeled polypropylene tube which was then sealed. Another solution was inoculated into each bottle for next immersion period. The collected solutions were analyzed for Ti, Al, V, Cu and Ni

using the inductively coupled plasma-mass spectrometer (ICP-mass, Hewlett Packard model 4500 series). The statistical significances of the influence of the experimental factors are tested and verified using Fisher analysis of variance (F test). If not specified, p values ≤ 0.01 were considered significant throughout the paper.

2.3. Surface analysis

After soaking in Hank/EDTA solution, specimens were removed at the appropriate immersion times (1, 4, and 16 days), sonicated three times in double distilled water and one time in absolute alcohol, dried using an Ar gas stream and immediately placed in a vacuum desiccator before surface examination by Auger electron spectroscopy (AES) and X-ray photoelectron spectroscopy (XPS). Shallower surface chemical analyses by XPS were carried out for various specimens after immersion. All analyses were carried out using VG Scientific ESCALAB 210 (analyzed area: 0.5 mm in diam.), operated at 12 KV and 20 mA in a pressure less than 10^{-8} mbar, using Mg Kα radiation. Measurements of binding energy in the range 0-1000eV were made at a "take-off" angle 45° with respect to the sample surface. High-resolution scans of Ti, Al, V, Cu, Ni, Na, S, Mg, Ca, P and O peaks were performed on selected specimens. The binding energy scale was calibrated by the C 1s peak at 284.6 eV. Besides, the surface composition of the reacted surface film was examined by AES (VG Microlab 310D). The vacuum pressure of AES was 2.9×10^{-9} mm Hg, and a monoenergetic electron beam with energy of 10 KV and current of 100 nA was employed. Selected specimens for depth profile examination were milled by argon ion bombardment at 3 KV and 9 mA. The oxide film thickness was calibrated by using the milling rate of Ta_2O_5 as standard.

3. Results

3.1. Ion release

After soaking in Hank/EDTA solution, the dissolution rates, derived from dividing the concentration of titanium ion measured per unit exposed surface area of the sample by the elapsed immersion time, are shown in Fig. 1, where a decrease in titanium release rate as a function of time is observed in all kind of specimens throughout the 0–8 day immersion periods ($p < 0.01$). After 8-day immersion, the dissolution rate of titanium becomes steady for all kinds of specimens. As shown in Fig. 1, 400 °C thermal passivation for both experimental materials (B2T and B8T) significantly reduce the dissolution rate compared to acid passivated and boiling water aged specimens (B2P, B2A, B8P and B8A) throughout the 32-day experimental period ($p < 0.0005$), whereas there is no statistical difference found between B2T and B8T during all immersion periods. For the nitric acid and aging passivation groups, the dissolution rate are significantly related to the experimental materials (B2 and B8) rather than the difference in passivation treatment. The titanium release rate for nitric acid and aging passivated specimens can generally be ranked in the following decreasing order: B2P/B2A, B8P/B8A with statistical significance ($p < 0.005$). The measured dissolution rate of titanium from B2P specimens are higher than B2A specimens throughout the experimental period, but no statistical differences are found in all immersion periods. Similarly, higher dissolution rate of titanium from nitric acid passivation are also observed for brazed specimens (B8P) compared to the aging treatment (B8A), but no

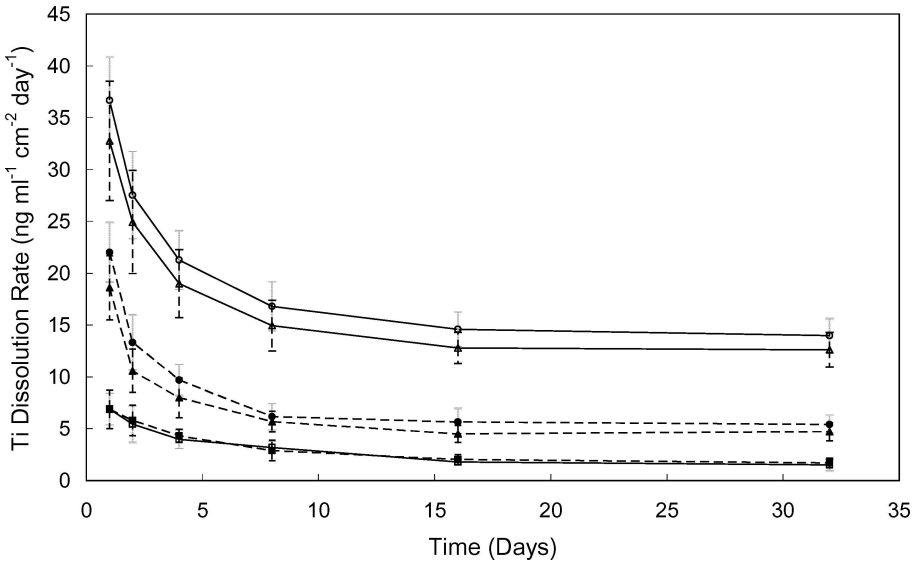

Figure 1 Dissolution rate (mean ± standard deviation) of titanium ion as a function of time for B2 and B8 specimens immersed in EDTA-containing Hank's solution. ○ B2P; □ B2T; △ B2A.; ● B8P; ■ B8T; ▲ B8A.

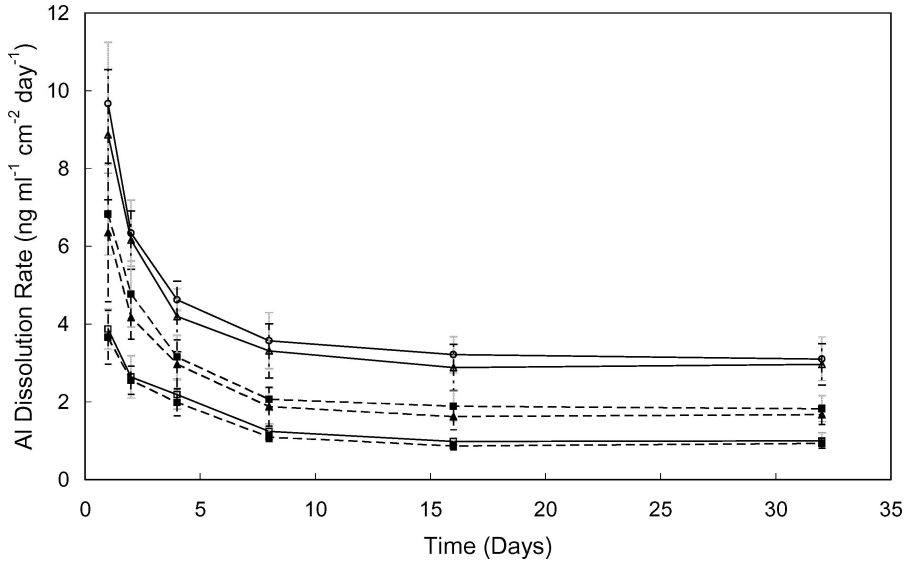

Figure 2 Dissolution rate (mean ± standard deviation) of aluminum ion as a function of time for B2 and B8 specimens immersed in EDTA-containing Hank's solution. ○ B2P; □ B2T; △ B2A.; ● B8P; ■ B8T; ▲ B8A.

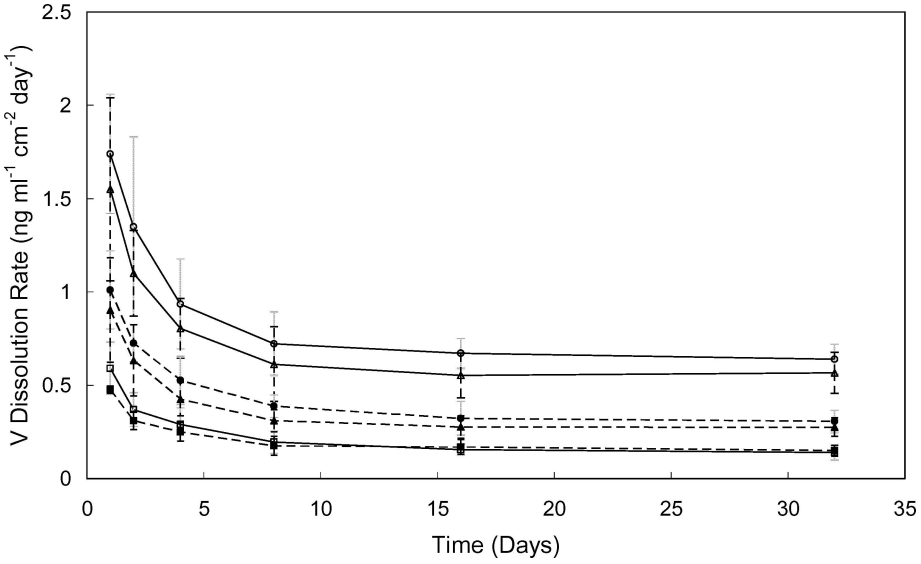

Figure 3 Dissolution rate (mean ± standard deviation) of vanadium ion as a function of time for B2 and B8 specimens immersed in EDTA-containing Hank's solution. ○ B2P; □ B2T; △ B2A.; ● B8P; ■ B8T; ▲ B8A.

statistical differences are found between the acid and aging treatment for the same experimental material.

The results of aluminum, vanadium, copper, and nickel dissolution rate are shown in Figs. 2–5, respectively. Likewise, there is a transient dissolution rate during the 0-8 day incubation period, and the dissolution rate of aluminum, vanadium, copper, and nickel from all groups of specimens becomes steady after immersion for 8 days. The effect of passivation treatments and experimental materials on the aluminum, vanadium, copper, and nickel release rates show the same tendency as the titanium. There are significant reductions in dissolution rate of aluminum, vanadium, copper, and nickel in 400 °C passivated specimens compared to the nitric acid and aging passivation groups throughout the 32-day experimental periods ($p < 0.01$), but no significant differences are found between B2T and B8T during all immersion periods. For nitric acid and aging passivation treatment, the release rates of aluminum, vanadium, copper, and nickel are also significantly related to the experimental materials rather than the passivation treatment throughout all immersion periods. The dissolution rate of aluminum, vanadium, copper, and nickel for nitric acid and aging specimens can generally be ranked in the following decreasing order: B2P/B2A, B8P/B8A ($p < 0.01$).

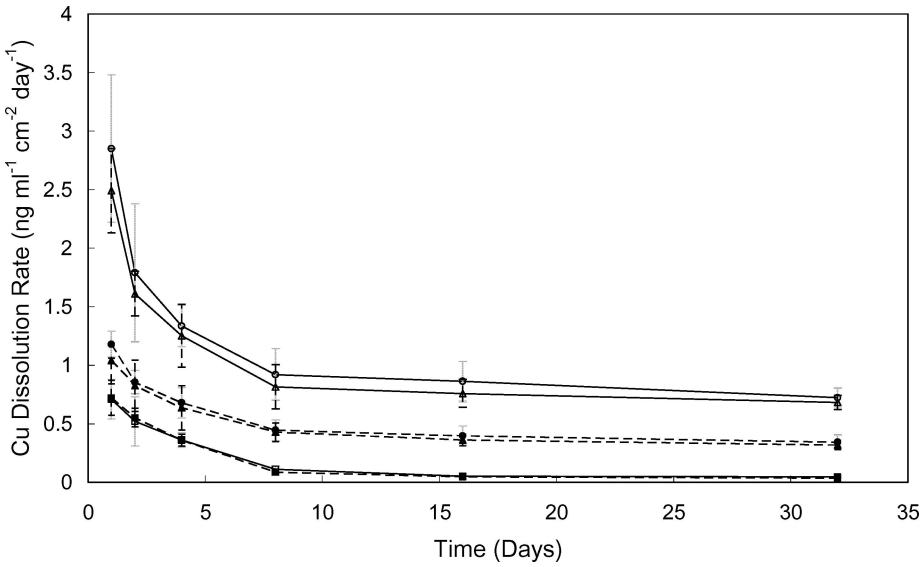

Figure 4 Dissolution rate (mean ± standard deviation) of copper ion as a function of time for B2 and B8 specimens immersed in EDTA-containing Hank's solution. ○ B2P; □ B2T; △ B2A.; ● B8P; ■ B8T; ▲ B8A.

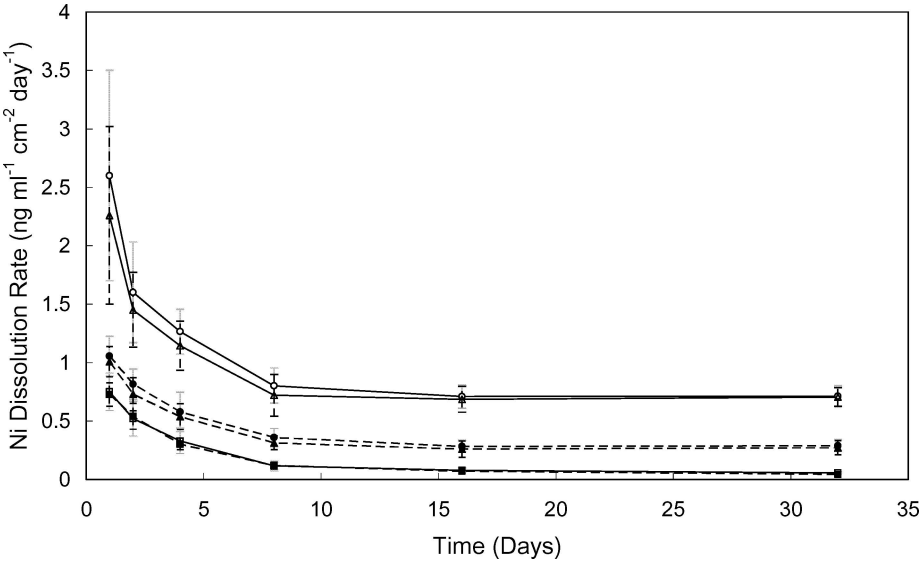

Figure 5 Dissolution rate (mean ± standard deviation) of nickel ion as a function of time for B2 and B8 specimens immersed in EDTA-containing Hank's solution. ○ B2P; □ B2T; △ B2A.; ● B8P; ■ B8T; ▲ B8A.

3.2. Characteristics of samples after immersion

3.2.1. XPS analysis

After immersion in Hank/EDTA solution, broad-range XPS spectra of nitric-acid passivated and autoclaved B2 (B2P) are shown in Fig. 6. The scans for 1, 4, and 16 days immersion are very similar, with consistent indication of the presence of Ti, Al, O, and C. In a more sensitive scale, the presence V, Ca, and P on the B2P specimens can be detected, but the peaks of Cu and Ni are not found in the XPS spectra. As shown in Fig. 7, the presence of P is observed on the B2P specimens by the P 2p3 peak at 133.3 eV after 1-day immersion. In high resolution scan, Ca is also detected on the surface of B2P specimens by the Ca 2p3 peak at 347.4 eV after soaking in Hank/EDTA solution for 1 day (as shown in Fig. 8). The existence of Ca and P are in the form of non-element because the binding energy of elemental Ca and P are 345.9 eV [26] and 130.2 eV [27], respectively. After soaking in Hank/EDTA solution, the broad-range XPS spectra of the 100 °C -aged B2 with autoclaving are very similar to B2P. XPS analysis of B2A is observed with the presence of Ti, O, C, and Al in the survey spectra, while V, Ca, and P can be detected in high resolution scan after 1-day immersion. The peaks of Cu and Ni are also not in a more sensitive scale. After immersed in Hank/EDTA solution, the results of XPS analysis of B2T are similar to B2P and B2A except for that the

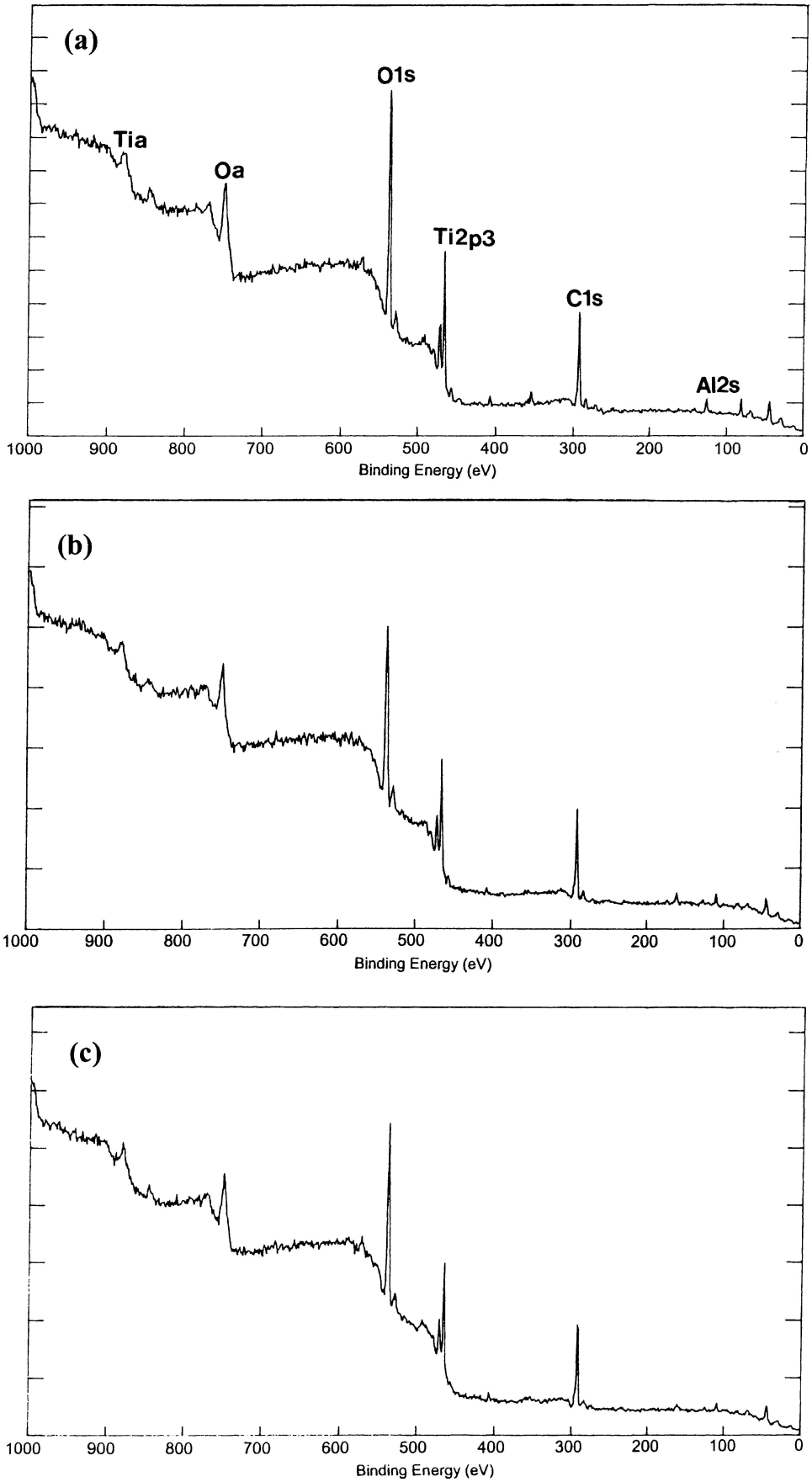

Figure 6 Broad-range XPS spectra of B2P specimen after immersion in Hank/EDTA solution for: (a) 1 day, (b) 4 days, and (c) 16 days.

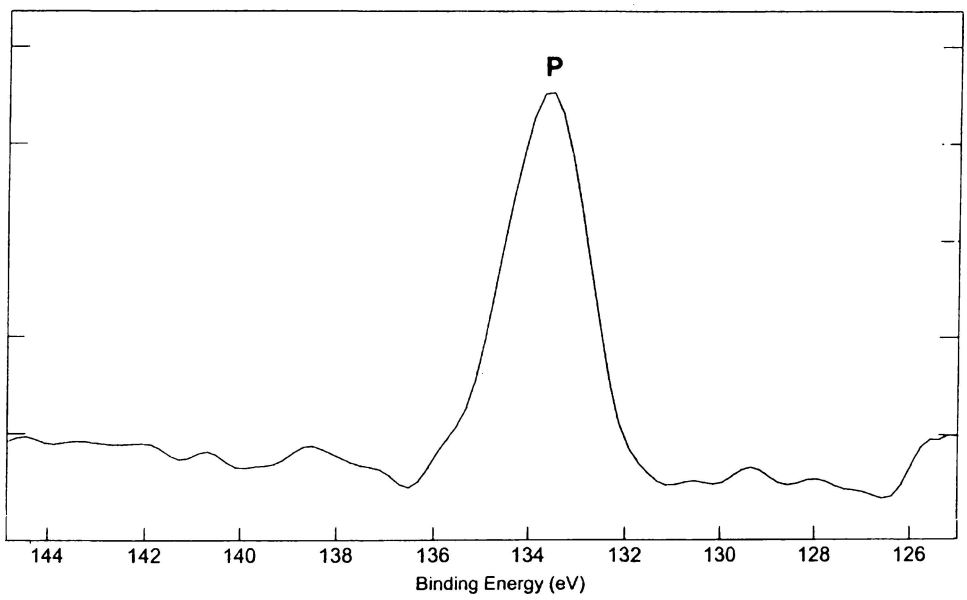

Figure 7 After immersion in Hank/EDTA solution for 1 day, the presence of P is observed at the surface of B2P specimen by the P 2p3 peak at 133.3 eV.

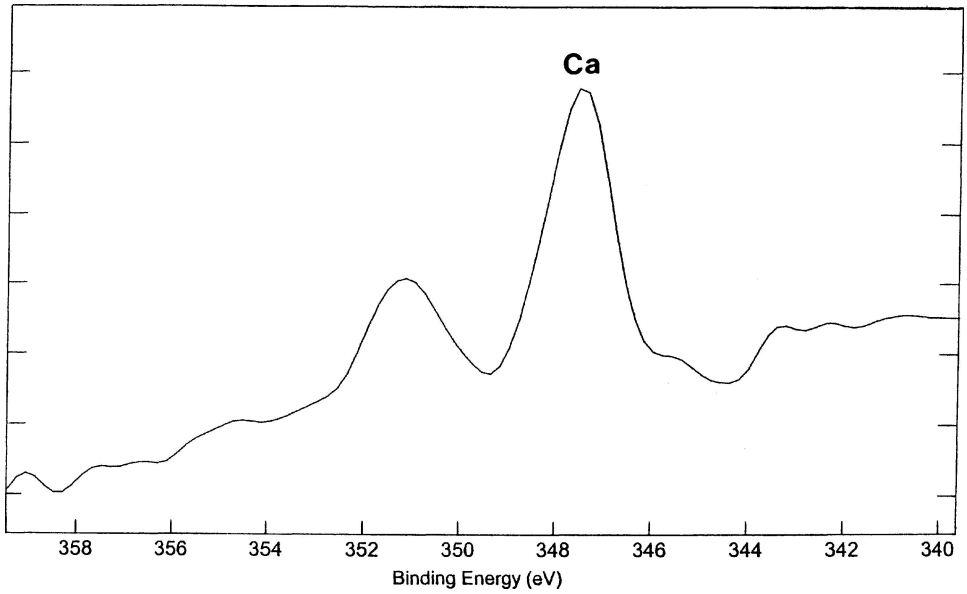

Figure 8 After immersion in Hank/EDTA solution for 1 day, the presence of Ca is observed at the surface of B2P specimen by the Ca 2p3 peak at 347.4 eV.

Cu and Ni are found in high resolution scan during all immersion periods.

After 1-, 4-, and 16- day immersion, the XPS scans of B8P and B8A are similar to B2P and B2A, with consistent indication of the presence of Ti, Al, O, and C. In a more sensitive scale, the existence of V, Ca, and P on the B8P and B8A specimens can be detected, but the peaks of Cu and Ni are not found in the XPS spectra. In high resolution scans, the non-elemental Ca and P are also observed on both B8P and B8A only after 1-day immersion in Hank/EDTA solution. After immersed in Hank/EDTA solution, the results of XPS analysis of B8T are similar to B8P and B8A except for that the Cu and Ni are found in high resolution scan during all immersion periods.

3.2.2. AES analysis

Fig. 9 shows the results of AES depth-profile chemical composition of the top surface of the B2P specimens after immersion in Hank/EDTA solution for 1 day. As shown in this figure, the outer phase of oxide film is composed of Ti, Al, O, Ca, and P, but the signal of V is found after 700 s sputtering. Similar spectra were found

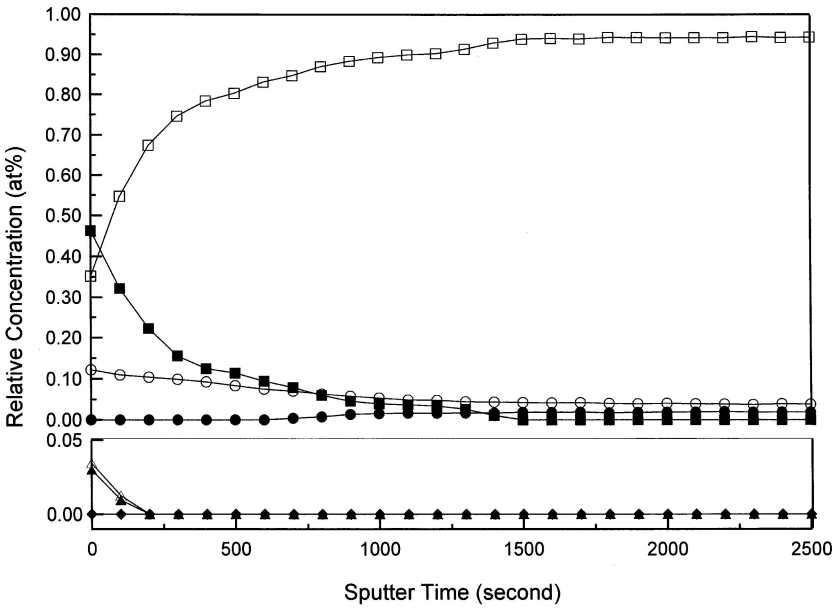

Figure 9 After immersion in Hank/EDTA solution for 1 day, AES depth-profile chemical composition with sputter time on the surface of the B2P specimen, and both of Cu and Ni are not found during depth profile process: □ Ti, ■ O, ○ Al, ● V, ◇ Cu, ♦ Ni △ Ca, ▲ P.

for the B2P samples immersed for 4 and 16 days. For all immersion periods, both of Cu and Ni are not found in the AES spectra of B2P during depth profile process. As shown in Fig. 9, the O signal has decreased to zero after 1400 s sputtering in the B2P after immersion in Hank/EDTA solution for 1 day, while the signals have decreased to zero after 1700 s and 1900 s sputtering in the B2P specimens soaked for 4 and 16 days, respectively. For B2T specimens, the AES depth-profile chemical composition are very similar to B2P. After soaking for 1 day, the reacted films of B2T is composed of Ti, Al, O, Ca, and P in the outer phase and V in the inner phase, but the existence of Cu and Ni are found in the outer phase of the reacted film. However, the reacted film contains less contents of Cu and Ni in the outer phase compared to the inner phase. The O signal decreases to zero after 1900 s sputtering in the B2T specimens after 1 day immersion. Similarly, the increase of depth-profile time of O signal decreasing to zero is consistent with longer immersion period (Table I). For B2A specimens, the AES chemical composition of top surface of B2A specimens is similar to the results of B2P specimens in Hank/EDTA solution. The reacted films is composed of Ti, Al, O, Ca, and P in the outer phase and V in the inner phase, and both of Cu and Ni are not found in the spectra of AES during depth profile process. Besides, the thickness of oxide film of the B2A increases with longer immersion periods, and the data of calibrated oxide thickness before and after immersion are shown in Table II.

After soaking in Hank/EDTA solution, the results of AES depth-profile chemical composition of the surface of B8P are similar to the corresponding results of B8P, and the reacted film of B2P is composed of Ti, Al, O, Ca, and P in the outer surface and V in the inner surface. For B8T specimens, AES chemical compositions of the surface after immersion for 1, 4, and 16 days are similar to the results of B2T. After immersion in Hank/EDTA solution, the AES depth-profile chemical composition of top surface of 100 °C-aged B8 (B8A) are similar to B2A during all immersion periods. As shown in Table II, the thicker oxide films have been formed on the surface of the specimens at longer immersion periods.

TABLE I After immersion in Hank/EDTA solution, the sputtering time (second) of oxygen signal decreasing to zero of specimens as a function of immersion period (day)

Immersion period	B2P	B2T	B2A	B8P	B8T	B8A
0	1100	1700	1300	1100	1800	1300
1	1400	1900	1500	1400	2000	1600
4	1700	2100	1800	1600	2100	1700
16	1900	2400	2000	1800	2300	2000

TABLE II After immersion in Hank/EDTA solution, the oxide thickness (nm) of specimens as a function of immersion period (day)

Immersion period	B2P	B2T	B2A	B8P	B8T	B8A
0	2.47	3.82	2.92	2.47	4.04	2.92
1	3.14	4.27	3.37	3.14	4.49	3.59
4	3.82	4.71	4.04	3.59	4.71	3.82
16	4.27	5.39	4.49	4.04	5.16	4.49

TABLE III EDS analyses of surface chemical composition (wt%) for typical B2 - and B8-series specimens without passivation and autoclaving treatments [28]

Materials	Ti	Al	V	Cu	Ni
B2	85.3	2.8	2.0	4.4	5.5
B8	86.7	3.3	2.7	3.6	3.7

4. Discussion

In order to diminish the intermetallic compound (Ti_2Cu) in brazed Ti6Al4V, the diffusion during brazing could substantially reduce the phase after 8 hr heat treatment [28]. According to ASTM protocol (F1148-88 and F1044-87), the porous coating on Ti6Al4V manufactured by 8 hr vacuum-brazed treatment show higher bonding strength and shear strength than 2hr treatment [24]. By EDS analysis, the chemical composition of vacuum-brazed Ti6Al4V are presented in Table III [28]. Comparing with 2hr brazed specimen (B2), the 8hr brazed specimen (B8) show a lower chemical composition (in wt%) of Cu and Ni. By the observation of optical microscopy [24], the brazing zone, consisted of Widmanstatten structure, increased from about 290 um (B2) to about 460 um (B8) in depth, and this could be explained by the diffusion of brazing elements (Cu and Ni) into the Ti6Al4V substrate. The material properties, such as chemical composition, microstructure and nano-surface characteristic, would influence the ion dissolution. This study examines the effects of heat-treated conditions (970 °C for 2 and 8 h) and surface treatments (34% nitric acid passivation, 400 °C heated in air, and aged in 100 °C de-ionized water) on the ion release and nano-surface characteristics of vacuum-brazed Ti6Al4V.

4.1. Effect of passivation treatments on ion release

Table IV show that the constituent elements (Ti, Al, V, Cu, and Ni) released for each group during the 0–1 day period. Thermal 400 °C passivation for both experimental materials significantly reduce the trace levels of constituent elements (Ti, Al, V, Cu, and Ni) compared to acid passivated and boiling water aged specimens during the 0–1 day period ($p < 0.001$), and the reduction of constituent releases for 400 °C passivated specimens could be observed throughout the 32-day experimental period. By 400 °C thermal treatment, both B2T and B8T specimens possess a thicker oxide thickness, lower contents of suboxide phases, and denser oxide structure [29], which could reduce ion release from implant in clinical use. Brwone and Gregson have found that the oxide films on the surfaces of Ti-6Al-4V treated by 400 °C in air for 45 min alloys belong to rutile structure by TEM [30]. In comparison, the oxide films passivated by nitric acid are the mixture of amorphous, anatase, and rutile structure in the same study of Brwone and Gregson. The rutile with more dense and closer packed structure could improve dissolution resistance in comparison with amorphous and anatase structure.

4.2. Effect of passivation treatments on Ca and P adsorption after immersion

Of the three types of passivation treatment [29], the 400 °C thermal treatment exhibits the lowest contents of suboxide and metallic elements and the thickest oxide by XPS analysis; however, this treatment cause the desorption of the basic OH group in the hydration layer on the surface of B2 and B8 (Table V). This phenomenon might reduce the ability of adsorbing species from the biological milieu because the ability of adsorption of species mainly depends on the existence of amphoteric OH groups in oxide film. After soaking in Hank/EDTA solution for 1 day, the reacted films of both 400 °C -treated B2 and B8 specimens also contain the non-elemental Ca and P in comparison with acid-passivated and boiling water-aged specimens. Furthermore, the presence of Cu and Ni in the top surface of B2T and B8T specimens does not change the ability of adsorption species (Ca and P) from the Hank/EDTA solution during immersion periods. The existence of Cu and Ni in oxide film is possible to change the properties of titanium oxide and furthermore to change the behavior of acidic and basic OH groups. In the study of Healy and Ducheyne [9], the amphoteric OH groups exist in the outer phase of titanium oxide by comparing high-resolution O 1s spectra with different take-off angle, and

TABLE IV Normalized concentration of constituent elements releases for each group during the 0–1 day period

Time of Immersion (days)	B2P	B2T	B2A	B8P	B8T	B8A
Ti	36.68	6.91	32.76	22.00	6.87	18.59
Al	9.67	3.87	8.87	6.83	3.65	6.36
V	1.74	0.59	1.55	1.01	0.48	0.90
Cu	2.85	0.71	2.49	1.18	0.72	1.04
Ni	2.60	0.75	2.26	1.05	0.73	1.01
Total (Ti + Al + V + Cu + Ni)	53.54	12.83	47.93	32.07	12.45	27.90

(Unit: ($ng/ml/cm^2$).

TABLE V Nano-surface properties by XPS analyses for the passivated specimens with autoclaving treatment [29]

	The relative contents (wt%) of titanium spectra				The relative contents (at%) of oxygen spectra		
Specimens	Suboxides ($Ti^{3+} + Ti^{2+}$)	Metallic Ti (Ti^0)	Titanium oxide (Ti^{4+})	Oxide Thickness (nm)	Ti—OH basic	OH acidic	O 1s
B2P	14.5	3.4	82.1	2.47	20.3	22.5	57.2
B2T	7.5	0.9	91.6	3.82	8.1	26.7	65.2
B2A	11.6	1.9	86.5	2.92	18.1	27.2	54.7
B8P	14.6	3.9	81.5	2.47	14.5	30.5	55.0
B8T	7.5	1.0	91.5	4.02	6.7	23.5	69.8
B8A	11.5	2.4	86.1	2.92	17.8	24.3	57.9

the presence of acidic and basic OH groups is derived from the hydrated titanium oxide exposed to ambient moisture. Hydration minimizes the surface potential by forming amphoteric OH sites. Although the existence of Cu and Ni are detected in the outer phase of oxide films of B2T and B8T specimens, we suggest that the existence of acidic and basic OH groups in the oxide film is mainly related to the Ti ions rather than Al, V, Cu, and Ni ions in the oxide film of specimens. The reason could be explained by that the higher contents of Ti ions might provide more bonding sites to form amphoteric OH groups.

4.3. Effect of immersion period on ion release and nano-surface characteristics after immersion

There is a significant reduction in constituent trace element release rate throughout the 0–8 day experimental period, and the transition period is observed for all kinds of specimens. By AES analysis, the oxide thickness of all kind of specimens increased with the immersion period (Table II). Dissolution of metal ions is a kinetic transport process, which govern the transportant of metal ions through the oxide layer, the hydrated layer and the concentration boundary layer (CBL) [13]. The driving force of the transport depends on the electrical field across the layers. The electrical field should be influenced by the electromotive force potential of the metals [31]. During immersion in the Hank/EDTA solution, oxidation of specimens occurs simulated with oxide dissolution. As the oxide thickens, the net potential differences across it decreases and the driven force is reduced. The thicker oxide may be the factor in the improved dissolution resistance.

During immersion in the Hank/EDTA solution, oxidation may be driven by an electric field established as a result of the potential drop across the oxide. In electrolyte solution, film thickening is explained on the basis of adsorption of anions on the oxide surface, whereby they create electric fields sufficiently high to allow the migration of metal (oxide) ions through the film to the oxide-electrolyte (oxide-metal) interface [32]. With increasing oxide thickness, the electric -field-assisted transport of metal ions through the oxide lattice decrease, and the thickening rate of oxide film slows down with longer immersion periods. As shown in Table VI, the thickening rates of B2P are 0.67 nm/day for 0–1 day, 0.15 nm/day for 1–4 day, and 0.06 nm/day for 4–16 day. Similar relation between the oxide thickening rates and immersion periods are also observed in the B2T, B2A, B8P, B8T, and B8A in Hank/EDTA solution. After immersion in Hank/EDTA solution, the oxide thickening rate of all kinds of specimens is shown in Table VI. During 0–1 day immersion, the thickening rate of acid passivated specimens is higher than 400 °C-treated specimens. There are three possible reasons for the phenomena: (1) Before immersion, the 400 °C-treated specimens contain higher oxide thickness compared to acidic passivated specimens. The electric field across higher oxide thickness will be reduced and the thickening rate is also decreased compared to thinner oxide films. (2) After 400 °C treatment, the specimens contain lowest content of basic OH group at the surface of oxide films. This reduction in the adsorption of anions can decrease the electric fields across oxide films, and also reduce the thickening rate compared to higher content of basic OH group on the surface of acidic passivated specimens. (3) In other studies [11, 30, 33], the oxide structure of 400 °C-treated Ti-6Al-4V belongs to rutile compared to anatase structure of oxide of acid passivaed Ti-6Al-4V. The rutile structure is denser and can reduce the ion release from 400 °C -treated Ti-6Al-4V against mixed rutile, anatase and amorphous structure for acid passivated Ti-6Al-4V. The denser structure would decrease the electric filed across the oxide film of oxide of thermally treated

TABLE VI After immersion in Hank/EDTA solution, the thickening rate (nm/day) of oxide thickness of specimens as a function of immersion period (day)

Immersion period	B2P	B2T	B2A	B8P	B8T	B8A
0–1	0.67	0.45	0.45	0.67	0.45	0.67
1–4	0.15	0.07	0.22	0.08	0.07	0.08
4–16	0.06	0.06	0.04	0.06	0.04	0.04

Ti-6Al-4V, and hence the thickening rate is also decreased.

4.4. Effect of surface modification on ion release

For acid passivated and boiling water aged treatment, the trace levels of constituent elements are significantly related to experimental materials (B2 and B8), but the statistical differences are not observed between the two methods of passivation process (P and A). These findings could be explained by that the 8 h brazed specimens containing lower contents of Ti_2Cu and higher contents of alpha-titanium by XRD analysis were thought to exhibit lower trace levels of constituent elements in Hank/EDTA solution. In the potentiodynamic study [25], the Ti_2Cu bulk specimens show worse corrosion resistance than commercial pure (CP) Ti and Ti-6Al-4V in 37 °C Hank solution with aeration by the bubbling with high purity oxygen. For the same experimental materials (B2 and B8), the autoclaving process could be the reason for no statistical differences found between nitric acid passivated and aging treated specimens. Wisbey *et al.* have found that 100 °C aged Ti-6Al-4V and titanium exhibited a substantial reduction in metal-ion release compared to nitric acid passivation during immersion in 0.17 M NaCl plus 2.7 mM EDTA [11], where γ-ray process was adopted for sterilization. In the present study, only a small advantage in ion release is found for the age passivated specimens against the acid passivated specimen. The advantage of age passivation at the boiling water temperature might be undermined since both the aged specimen and the acid passivated specimen were subject to the high-temperature 121 °C steam sterilization.

4.5. Effect of surface modification on nano-surface characteristics after immersion

After soaking in Hank/EDTA solution, the adsorption of non-elemental Ca and P are observed both on the surfaces of B2 and B8 with the three different passivation treatment by XPS analysis, and the adsorption of Ca and P should be derived from the formation of amophertic OH groups in oxide films. Meanwhile, the magnitude of these peaks increases from the reflection of shallower angles of incidence, suggesting a high concentration of those groups at the outermost oxide surface [33]. In high resolution scans of oxygen spectra [16], the basic and acidic OH groups have been observed in the nano-surface composition of B2 and B8 specimens with three different passivated treatments, and these suggest that B2 and B8 specimens would occur the similar oxide films/solution reaction. By surface modification, the specimens have changed their surface chemisteries (elemental composition in metals) and microstructures (Ti_2Cu and α-titanium), but the B2 and B8 specimens show the similar nano-surface characteristics after immersion in Hank/EDTA solution.

4.6. The proposed mechanisms of governed ion dissolution

As shown in Fig. 10, thicker oxide film and lower ion release rate of B2P have been observed at longer immersion periods, and the same tendency is also found in the other groups of specimens. The results support that the dissolution comes from the transport of ions from the metal through the oxide film. Healy and Ducheyne proposed the rate-limiting step for a titanium-electrolyte was the hydrolysis of the oxide [13]. However, our present study does not support their

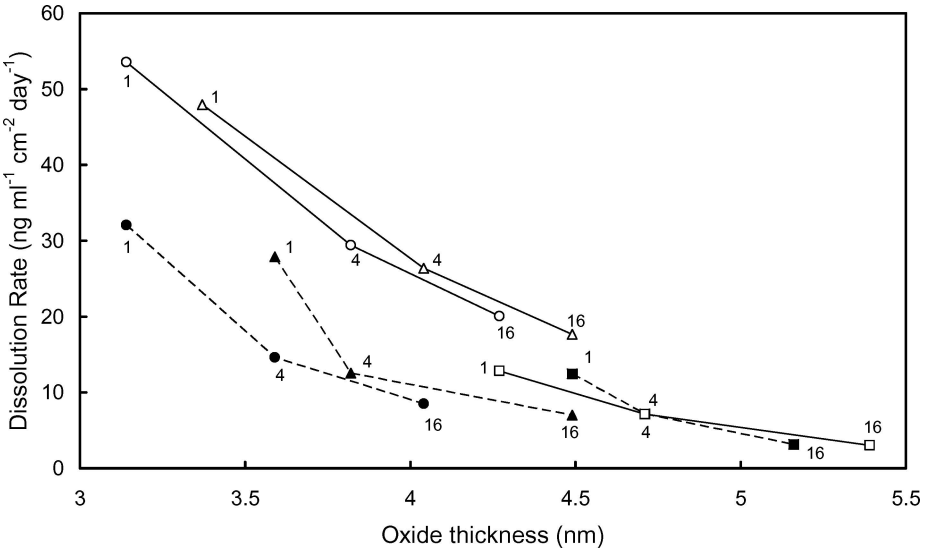

Figure 10 Correlation of total ion (Ti+Al+V+Cu+Ni) dissolution rate of variously treated specimens with the oxide thickness during immersion. The digit in the figure denotes the days of immersion. ○ B2P; □ B2T; △ B2A.; ● B8P; ■ B8T; ▲ B8A.

TABLE VII Surface chemical composition (wt%) by XPS analyses for passivated specimens with autoclaving treatment [29]

Immersion period	B2P	B2T	B2A	B8P	B8T	B8A
Ti	85.7	76.3	85.4	84.2	73.1	84.0
Al	11.3	11.3	11.9	13.0	14.8	12.9
V	3.0	2.2	2.7	2.8	3.2	3.1
Cu	Nil	5.8	Nil	Nil	5.0	Nil
Ni	Nil	4.4	Nil	Nil	3.9	Nil

mechanism. Because the B2T and B8T specimens contain the elements of Cu and Ni in the nano-surface oxides (Table VII) [29], B2P, B2A, B8P and B8A specimens contain nil Cu and Ni by XPS analysis. However, the dissolution rates of these elements in B2T and B8T specimens were lower than that in B2P, B2A, B8P and B8A (Figs. 4 and 5). Besides, the initial oxide thickness of B2T, B8T, B2P, B2A, B8P and B8A correlates inversely proportional to the dissolution rates of Cu and Ni in these specimens. This implies that the rate-limiting step in ion dissolution of titanium alloy can be best explained by the metal-ion transport through the thickness of oxide film and not the hydrolysis of the oxides.

5. Conclusions

In conclusion, the results presented in this study revealed improvement of ion release of 8 hr brazed specimens compared with B2 in Hank/EDTA solution. It is suggested that reduced Ti_2Cu and increased α-titanium structure in brazed Ti-6Al-4V could improve ion release resistance exposure to simulated body fluid. Of the three passivated treatments, 400 °C thermal treatment for both B2 and B8 exhibits a substantial reduction in the constituent release compared to the acid passivated and water aged treatment. The constituent element release rate decrease with time for all kinds of specimens throughout the 0–8 day experimental period. The thicker oxides may be the factor in the improved dissolution resistance. Of the three passivated treatment, the 400 °C treatment show the lower contents of amphoteric OH groups in oxide film for both B2 and B8 specimens, but the adsorption of non-elemental Ca and P were also observed on the surfaces of B2T and B8T. By AES depth-profile analysis, the oxide films of all kinds of specimens thicken with the longer immersion periods, and increasing oxide thickness reduce the constituent element release rate form specimens. The thickening rate of oxide film slows down with longer immersion periods, and this could be explained by the decrease of electric-field-assisted transport of metal ions through the oxide lattice with increasing oxide thickness. In this study, the AES and XPS are carried out to evaluate the elemental composition and chemical state of nano-surface characteristics of specimens. The structure and morphology of nano-surface characteristics need be further studied by transmission electron microscopy (TEM) and atomic force microscopy (AFM).

Acknowledgments

This study was supported by grant NSC-91-2213-E-242-001 from the National Science Council, Taiwan.

References

1. J. GALANTE, W. ROSTOKER, R. LUECK and R. D. RAY, *J. Bone Joint Surg.* **53A** (1971) 101.
2. T. ALBREKTSSON, P. I. BRANEMARK, H. A. HANSSON, B. KASEMO, K. LARSSON, I. LUNDSTORM, D. H. MCQUEEN and R. SKALAK, *Ann. Biomed. Eng.* **11** (1983) 1.
3. B. KASEMO, *J. Prosthet Dent.* **49** (1983) 832.
4. P. A. MAEUSLI, P. R. BLOCH, V. GERET and G. STEINEMANN, in "Biological and Biomedical Performance of Biomaterials," edited by P. Christel, A. Meunier, and A. J. C. Lee (Elsevier Amsterdam, 1986) p. 57.
5. C. JOHANSSON, J. LAUSMAA, M. ASK, H-A. HANSSON and T. ALBREKTSSON, *J. Biomed. Eng.* **11** (1989) 3.
6. J. LAUSMAA, M. ASK, U. ROLANDER and B. KASEMO, *Mater. Res. Symp. Proc.* **110** (1989) 647.
7. J. LAUSMAA, L. MATTSSON, U. ROLANDER and B. KASEMO, *Mater. Res. Symp. Proc.* **55** (1986) 351.
8. J. LAUSMAA, B. KASEMO and H. MATTSSON, *Appl. Surf. Sci.* **44** (1990) 133.
9. K. HEALY and P. DUCHEYNE, *Biomaterials*, **13** (1992) 553.
10. M. BROWNE, P. J. GERGSON and R. H. WEST, *J. Mater. Sci. Mater. Med.* **7** (1996) 323.
11. A. WISBEY, P. J. GERGSON, L. M. PETER and M. TUKE, *Biomaterials*, **12** (1991) 470.
12. P. DUCHEYNE and K. E. HEALY, in "The Bone–Biomaterial Interface," edited by J. E. Davies (University of Toronto Press, 1991) p. 62.
13. K. E. HEALY and P. DUCHEYNE, *J. Biomed. Mater. Res.* **26** (1992) 319.
14. R. J. SOLAR, S. R. POLLACK and E. KOROSTOFF, 'in "Corrosion and Degradation of Implant Materials," edited by B. C. Syrett and A. Acharya (American Society for Testing and Materials, Philadelphia, 1979) p. 161.
15. E. CHANG and T. M. LEE, *Biomaterials* **23** (2002) 2917.
16. R. M. PILLAR, *J. Biomed. Mater. Res. Appl. Biomaterials* **21 A1** (1987) 1.
17. J. J. CALLAGHAN, *J. Bone and Joint Surgery* **75A** (1993) 299.
18. J. D. BOBYN, R. M. PILLAR, H. U. CAMERON and G. C. WEATHERLY, *Clin. Orthop.* **150** (1980) 263.
19. J. J. CALLAGHAN, R. D. HEEKIN, C. G. SAVORY, S. H. DYSTAR and W. J. HOPKINSON, *Clin. Orthop.* **282** (1992) 132.
20. S. YUE, R. M. PILLAR and G. C. WEATHERLY, *J. Biomed. Mater. Res.* **18** (1984) 1043.
21. S. D. COOK, F. S. GEOGETTE, H. B. SKINNER and R. J. HADDAD, *ibid.* **18** (1984) 497.
22. S. D. COOK, N. THOMGPERDA, R. C. ANDERRSON and R. J. HADDAD, *ibid.* **22** (1988) 287.
23. C. A. STUBBINGTON and A. W. BOWEN, *J. Mat. Sci* **9** (1974) 941.
24. C. H. YEH, Master Thesis, (National Cheng Kung University, 1995).
25. E. CHANG and C. H. CHEN, *J. Mater. Eng. Perf.* **6** (1997) 792.

26. D. BRIGGS and M. P. SEAH, in "Practical Surface Analysis, vol. 1, 2nd ed., Auger and X-ray Photoelectron Spectroscopy," edited by D. Briggs and M. P. Seah (Chichester: Wiley, 1990) p. 605.
27. D. BRIGGS and M. P. SEAH, in "Practical Surface Analysis, vol. 1, 2nd ed., Auger and X-ray Photoelectron Spectroscopy" (Chichester: Wiley, 1990) p. 603.
28. T. M. LEE, E. CHANG and C. Y. YANG, *J. Mat. Sci. Maert. Med.* **9** (1998) 429.
29. *Idem. ibid.* **9** (1998) 439.
30. M. BROWNE and P. J. GERGSON, *Biomaterials* **15** (1994) 894.
31. D. A. JONES, in "Principles and prevention of corrosion" (Macmillan Publishing Co., New York, 1992) p. 42.
32. A. M. SHAMS and A. A. HAMMOUD, *Thin Solid Films* **167** (1988) 269.
33. M. BROWNE, P. J. GERGSON and R. H. WEST, *J. Mater. Sci. Mater. Med.* **7** (1996) 323.

Received 17 March 2005
and accepted 5 September 2005